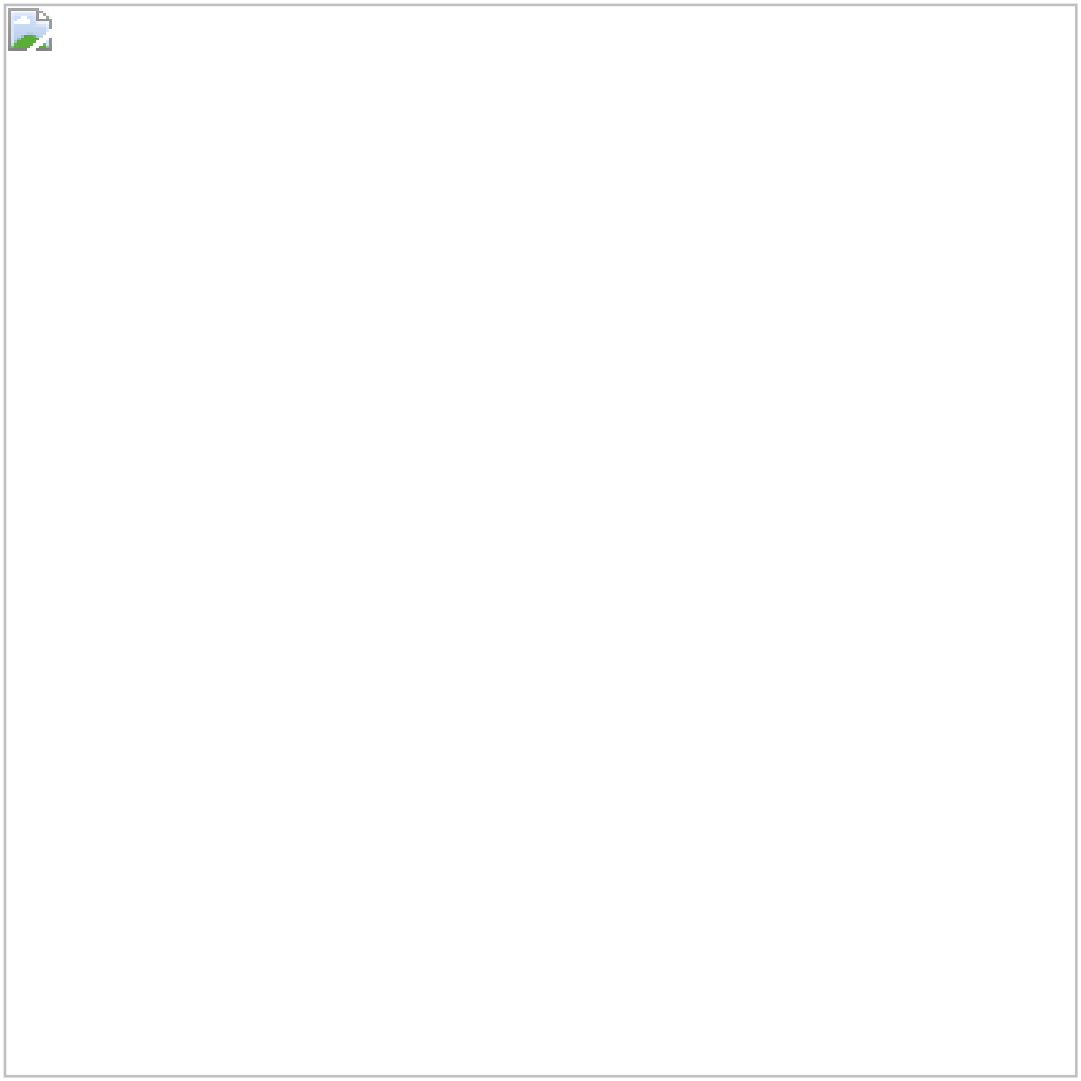

Wing Kinematics in a Hovering Dronefly Minimize Power Expenditure

Authors: Wu, J. H., and Sun, M.

Source: Journal of Insect Science, 14(159) : 1-8

Published By: Entomological Society of America

URL: https://doi.org/10.1093/jisesa/ieu021

RESEARCH

Wing Kinematics in a Hovering Dronefly Minimize Power Expenditure

J. H. Wu[1,2] and M. Sun[3]

[1]School of Transportation Science and Engineering, Beihang University, Beijing, China
[2]Corresponding author, e-mail: buaawjh@buaa.edu.cn
[3]Ministry-of-Education, Key Laboratory of Fluid Mechanics, Beihang University, Beijing, China

Subject Editor: Henry Hagedorn

J. Insect Sci. 14(159): 2014; DOI: 10.1093/jisesa/ieu021

ABSTRACT. When an insect hovers or performs constant-speed flight, its wings flap at certain amplitude, frequency, angle of attack, etc., and the flight is balanced (vertical force equals to the weight, and horizontal force and pitch moment are zero). It is possible that when some other sets of values of wing kinematical parameters are used, the force and moment balance conditions can still be satisfied. Does the wing kinematics used by a constant-speed flying insect minimize the power expenditure? In this study, whether the wing kinematics used by a freely hovering dronefly minimizes its energy expenditure was investigated. First, the power consumption using the set of values of wing kinematical parameters that was actually employed by the insect was computed. Then, the kinematical parameters were changed while keeping the equilibrium flight conditions satisfied, and the power consumption was recalculated. It was found that wing kinematical parameters used by the freely hovering dronefly are very close to that minimize its energy consumption, and they can ensure the margin of controllability from hovering to maneuvers. That is, slight change of wing kinematical parameters did not cause significant change of the specific power (maintained a relatively small value).

Key Words: insect, hovering, power expenditure, Navier–Stokes simulation

When an insect hovers or performs constant-speed flight, its wings flap at certain amplitude, frequency, angle of attack, etc.; the vertical component of the aerodynamic force of the wings balances the weight, the thrust overcomes the body drag, and the aerodynamic moment about the center of mass of the insect is zero. It is possible that when some other sets of values of wing kinematical parameters are used, the force and moment balance conditions can still be satisfied, and the insect can still perform constant-speed flight or hovering. For example, when the stroke amplitude is decreased, but the angle of attack is increased, by certain amount (with some adjustments on the mean stroke angle), the same vertical force, thrust, and moment (zero) can be produced. That is, an insect could perform constant-speed flight or hovering using different combinations of wing kinematical parameters. Although different combinations of wing kinematical parameters might give the same aerodynamic forces and moments, the energy consumption is different in general. It is of great interest to ask the question "Does the wing kinematics used by a hovering (or constant-speed flying) insect minimize the power expenditure?" In this study, this question is addressed.

Power consumption in insect flight was studied using theoretical, numerical, and experimental method (e.g., Ellington 1984a, 1984b; Dudley and Ellington 1990; Sun and Tang 2002; Sun and Du 2003; Liu and Aono 2004; Fry et al. 2005; Zhao and Deng 2009). Early works used the blade-element theory combined with vortex theory or momentum theory to compute the aerodynamic power (Ellington 1984a, Dudley and Ellington 1990). Because the method did not take into account some major aerodynamic mechanisms, such as the leading-edge vortex, the computed power was much lower than that was expected from measurements of oxygen consumption. Recent studies on power consumption employed computational method based on computational fluid dynamics (CFD) (Sun and Tang 2002, Sun and Du 2003, Liu and Aono 2004) or experimental method of measuring the aerodynamic force and torque of the wings using a dynamically scaled robotic wing model (Fry et al. 2005, Zhao and Deng 2009). Using the wing kinematics of flying insects, these numerical and experimental methods gave a vertical force that approximately balanced the insect weight and a horizontal force and a moment about the center of mass that were close to zero. This indicated that the aerodynamic forces and moment were computed or measured with good accuracy, and hence, the aerodynamic power could be correctly estimated.

In this study, we employ the CFD method to calculate the aerodynamic power and investigate whether the wing kinematics used by a freely hovering dronefly minimizes its energy consumption. Wing kinematical parameters of freely hovering droneflies (*Eristalis tenax*) were measured recently by our group (Liu and Sun 2008). We first compute the power consumption using the set of wing kinematical parameters that is actually employed by the insect. We then change the kinematical parameters while keeping the equilibrium flight conditions satisfied and recalculate the power consumption. With the computed data, the question raised above can be addressed.

Materials and Methods

The Wings, the Coordinate Systems, and the Wing Kinematics. The wing planform used (Fig. 1) is approximately the same as that of a dronefly (Liu and Sun 2008). On the basis of measurement by Walker et al. (2010) and calculation by Du and Sun (2012) on the effect of wing deformation on aerodynamic forces, it is showed that as a first approximation, the deformable wing could be modeled by a rigid flat-plate wing with its angle of attack being equal to the local angle of attack at the radius of second moment of wing area. Thus, we assume that wings are rigid flat-plate wings; the wing section is modeled as a flat plate with rounded leading and trailing edges and the thickness of which is 3% c (c is the mean chord length of the wing). In accordance with our past study (Wu et al. 2009), body movement is very little and can be neglected for a hovering dronefly. The radius of the second moment of wing area (r_2) is computed as $0.55R$, where R is the wing length (the mean flapping velocity at span location r_2 is used as reference velocity in this study).

To clearly describe the wing motion and to resolve the force components, three coordinate systems are used. Two are inertial coordinate systems, $OXYZ$ and $OX_eY_eZ_e$. For $OXYZ$, the origin O is at the wing base (Fig. 2A); its X-Y plane coincides with the stroke plane (Fig. 2A and B), and the Z direction is vertical to stroke plane. The coordinate

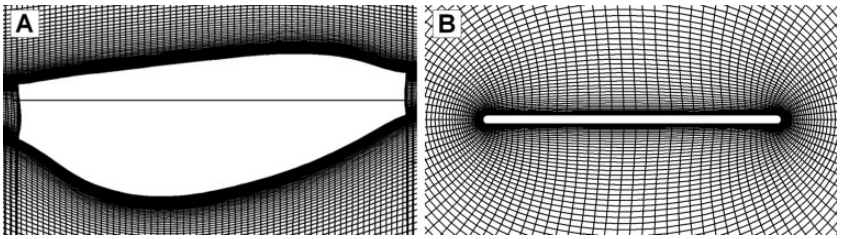

Fig. 1. Portions of the computation grid of the dronefly wing (A) in the plane of wing planform and (B) in a sectional plane.

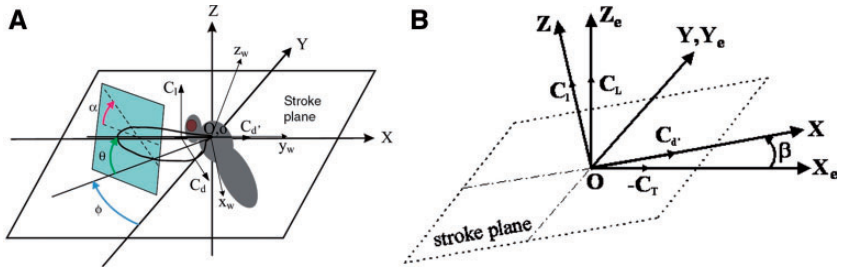

Fig. 2. Definitions of the angles of a flapping wing (β, stroke plane angle; ϕ, the positional angle; α, the geometrical angle of attack; θ, the stroke deviation angle) and the coordinate systems (inertial coordinate systems *OXYZ* and $OX_eY_eZ_e$; body-fixed coordinate system $ox_wy_wz_w$).

system $OX_eY_eZ_e$ has the same origin as the coordinate system *OXYZ*, its Y_e-axis coincides with the y-axis, and X_e-Y_e plane is the horizontal plane (Fig. 2B). The third is the body-fixed coordinate system $ox_wy_wz_w$. It has the same origin as the two inertial coordinate systems, but it rotates with the wing. The x_w-axis is parallel to the wing chord, and the y_w-axis is on the pitching-rotation axis of the wing (Fig. 2A).

The stroke plane angle (β), the stroke deviation angle (θ), the geometrical angle of attack (α), and the positional angle (ϕ) of a wing are defined as in Figure 2. Based on the measured data of the insect (Liu and Sun 2008), ϕ, α, and θ can be approximated by simple functions in the following. ϕ can be approximated by a simple harmonic function

$$\phi = \bar{\phi} + 0.5\Phi\sin(2\pi nt) \tag{1}$$

where n is the wing-beat frequency, $\bar{\phi}$ the mean stroke angle, and Φ the stroke amplitude; $\bar{\phi}$ and Φ are defined as follows: $\bar{\phi} = (\phi_{max} + \phi_{min})/2$, $\Phi = \phi_{max} - \phi_{min}$, where ϕ_{max} and ϕ_{min} are the maximum and minimum values of ϕ, respectively (see Ellington 1984b). The angle of attack of the wing (α) takes a constant value during the down- or upstroke translation (the constant value is denoted by α_d for the downstroke translation and α_u for the upstroke translation); around stroke reversal, the wing flips and α change with time, also according to the simple harmonic function. The function representing the time variation of α during the supination at mth cycle is:

$$\alpha = \alpha_d + a\left\{(t - t_1) - \frac{\Delta t_r}{2\pi}\sin\left[\frac{2\pi(t - t_1)}{\Delta t_r}\right]\right\},\ t_1 \le t \le t_1 + \Delta t_r \tag{2a}$$

where Δt_r is the time duration of wing rotation during the stroke reversal and a is a constant:

$$a = (180^\circ - \alpha_u - \alpha_d)/\Delta t_r \tag{2b}$$

t_1 is the time when the wing-rotation starts:

$$t_1 = mT - 0.5T - \Delta t_r/2 \tag{2c}$$

The expression of the pronation can be written in the same way.

Finally, the time variation of the deviation angle can be approximately represented by a simple harmonic function

$$\theta(t) = \theta_0 + \theta_1\sin(2\pi nt) \tag{3}$$

where θ_0 and θ_1 are the mean deviation angle and the amplitude of deviation angle, respectively.

Evaluation of Aerodynamic Forces and Mechanical Power. Under hovering flight conditions, Aono et al. (2008) and Yu and Sun (2009) showed that interaction between wing and body was negligibly small: the aerodynamic force in the case with the body–wing interaction was <2% different from that without body–wing interaction. Although the left and right wings might interact via a "clap and fling" mechanism, this mechanism is irrelevant in this study because of small stroke amplitude. Therefore, in the present CFD model, the body is neglected, and only the flows around one wing are computed (the aerodynamic forces produced by the other wing are derived from the results of the computed wing).

The flow equations (the Navier–Stokes equations) and solution method used in this study are the same as those described in Sun and Tang (2002) and Sun and Du (2003). In the method, the time derivatives of the momentum equations are differenced using a second-order, three-point backward difference formula. To solve the time-discretized momentum equations for a divergence free velocity at a new time level, a pseudotime level is introduced into the equations, and a pseudotime derivative of pressure divided by an artificial compressibility constant is introduced into the continuity equation. The resulting system of equations is iterated in pseudotime until the pseudotime derivative of pressure approached zero, and, thus, the divergence of the velocity at the new time level approaches zero. The derivatives of the viscous fluxes in the momentum equation are approximated using second-order central differences. For the derivatives of convective fluxes, upwind differencing based on the flux-difference splitting technique is used. A third-order upwind differencing is used at the interior points, and a second-order upwind differencing is used at points next to boundaries.

Boundary conditions are as follows. For the far-field boundary condition, at inflow boundary, the velocity components are specified as free-stream conditions, whereas pressure is extrapolated from the interior; at the outflow boundary, pressure is set equal to the free-stream static pressure, and velocity is extrapolated from the interior. On the

wing surface, impermeable wall and nonslip conditions are applied, and the pressure is obtained through the normal component of the momentum equation written in the moving grid system.

Once the flow equations are numerically solved, the fluid velocity components and pressure at discretized grid points for each time step are available. The aerodynamic forces and moments acting on the wing are calculated from the pressure and the viscous stress on the wing surface. The inertial moments due to the acceleration of the wing mass are calculated analytically.

The lift (l) is the component of the total aerodynamic force perpendicular to the translational velocity of the wing (defined below), i.e., perpendicular to the stroke plane, and is positive when it is in the positive Z direction (Fig. 2A). The drag (d) is the component of the total aerodynamic force parallel to the translational velocity and is positive when directed opposite to the direction of the translational velocity of the downstroke (Fig. 2A). The X component of d is denoted as d', and $d' = d\cos\phi$. Resolving l and d' into the z_e and x_e-axes, we obtain the vertical force (V) and the thrust (H), respectively (Fig. 2B):

$$V = l\cos\beta + d'\sin\beta \quad (4a)$$

$$H = l\sin\beta - d'\cos\beta \quad (4b)$$

The pitch moment of the total aerodynamic force about the center of mass of the insect is denoted by N. V, H, l, d, and d' are nondimensionalized by $0.5\rho U^2 S$ and N by $0.5\rho U^2 Sc$, where ρ is the fluid density, S is the wing area, c is the mean chord length of wing, and U is the mean flapping velocity at span location r_2, defined as $U = 2\Phi n r_2$, and the corresponding coefficients of these forces are denoted as follows: C_V, C_H, C_N, C_l, C_d, and $C_{d'}$.

The aerodynamic and inertial moments about the wing root are denoted as $\mathbf{M}_a$ and $\mathbf{M}_i$, respectively. The mechanical power of a wing (P) can be easily calculated:

$$P = (\mathbf{M}_a + \mathbf{M}_i)\cdot\Omega \quad (5)$$

where $\mathbf{\Omega}$ is the angular velocity vector of the wing. Let $P_a = \mathbf{M}_a\cdot\mathbf{\Omega}$ and $P_i = \mathbf{M}_i\cdot\mathbf{\Omega}$ be the aerodynamic and inertial power, respectively; thus $P = P_a + P_i$. The power is nondimensionalized by $0.5\rho U^3 S$, giving the aerodynamic, inertial, and total power coefficients as $C_{P,a}$, $C_{P,i}$, and C_P, respectively.

Before proceeding to compute the flows for obtaining the solution that represents the hover flight, we conducted grid resolution test to give some quantitative assessment of the accuracy of the aerodynamic force calculation. Three grids for the hawkmoth wing were considered: 27 by 27 by 32 (in the normal direction of the wing surface, around the wing section, and in the spanwise direction of the wing, respectively; first layer grid thickness was $0.003c$), 53 by 53 by 63 (first layer grid thickness was $0.001c$) and 107 by 107 by 126 (first layer grid thickness was $0.0005c$). Note that in each refinement, the grid dimension in each direction was approximately doubled. In the normal direction, the outer boundary was set at 20 chord lengths from the wing and in the spanwise direction; the boundary was set at six chord lengths from the wing. Portions of the dense grid (107 by 107 by 126) are shown in Figure 1. The nondimensional time step was 0.02 (nondimensionalized by c/U; the effect of time step value was studied, and it was found that a numerical solution effectively independent of the time step was achieved if the time step value was < 0.02). Calculations were performed using the above grids for the model dronefly wing in flapping motion (α_d, α_u, and $\bar{\phi}$ are 41.8, 41.8, and 2.5°, respectively).

For a clear description of the results, the time in a cycle is expressed as a nondimensional parameter, $\hat{t}$, such that $\hat{t} = 0$ at the start of the downstroke and $\hat{t} = 1$ at the end of the subsequent upstroke. The computed lift (C_L), drag (C_D), and pitching moment (C_M) coefficients are shown in Figure 3. It is observed that the first grid refinement produces a relatively large change in the results, but the second grid refinement

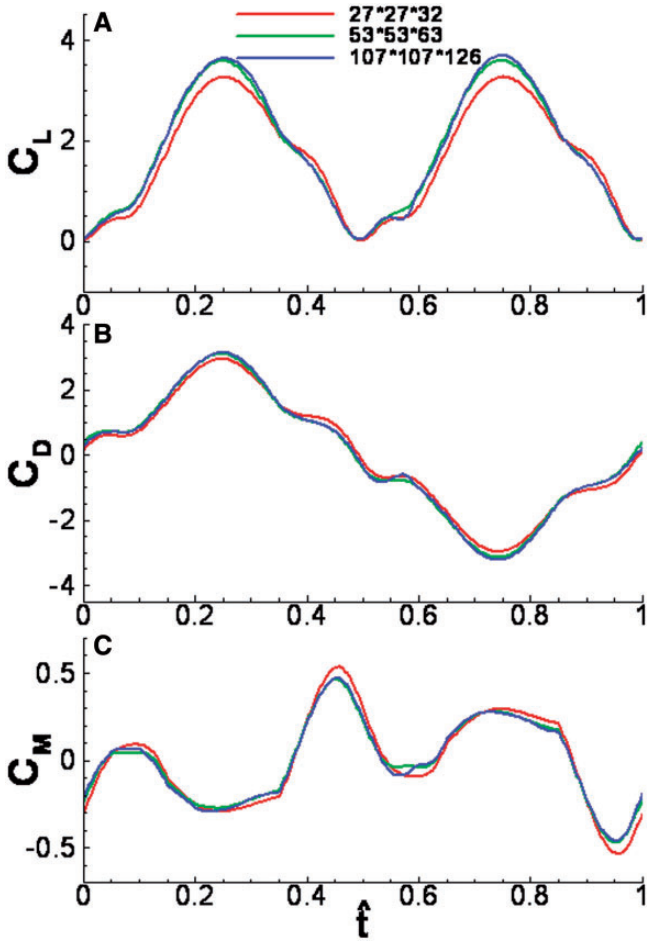

Fig. 3. Time courses of the lift (C_L), drag (C_D), and pitching moment (C_M) coefficients of the wing of dronefly at hovering flight for different grids.

produces very small change in the results. By the first grid refinement (from grid 27 by 27 by 32 to 53 by 53 by 63), the mean magnitudes of change in C_L, C_D, and C_M are 0.195, 0.142, and 0.034, respectively, and the values for the second grid refinement (from grid 53 by 53 by 63 to grid 107 by 107 by 126) are 0.045, 0.042, and 0.011, respectively. The ratio between the changes in C_L, C_D, and C_M is about 1:4, as expected for the second-order method. Let us use the above data to give an estimate of the accuracy of the solution obtained by grid (107 by 107 by 126). Suppose that the grid is further refined (doubling the grid dimension in each direction), one could expect that the changes in C_L, C_D, and C_M would be about 0.011 ($0.045/4 = 0.011$), 0.01 ($0.042/4 = 0.01$), and 0.003 ($0.011/4 = 0.003$), respectively. On the basis of the 1/4-convergence ratio, we could estimate that the solution by grid 107 by 107 by 126 has errors in C_L, C_D, and C_M as 0.015 ($0.011 \times [4/3] = 0.015$), 0.013 ($0.01 \times [4/3] = 0.013$), and 0.004 ($0.003 \times [4/3] = 0.004$), respectively. The mean C_L, C_D, and C_M are 1.831, 1.827, and 0.195, respectively. Therefore, it is estimated that when using the grid 107 by 107 by 126, the numerical discretization and convergence errors in the mean C_L, C_D, and C_M are <2.0%. The grid 107 by 107 by 126 is used for the present flow computations.

Flight Data. Flight data for the hovering dronefly are taken from Liu and Sun (2008). Table 1 lists the general morphological data; the data include m (insect mass), m_{wg} (mass of one wing), R, c, r_2, S, $I_{x,w}$, $I_{y,w}$, $I_{z,w}$ (moments of inertia of a wing about x_w, y_w, and z_w axes, respectively), and $I_{xz,w}$ (product of inertia of a wing). Table 2 lists the wing-kinematic data (Φ, n, α_d, α_u, $\bar{\phi}$, θ_0, θ_1, Δt_r, β).

Table 1. Morphological data of wing

m (mg)	m_{wg} (mg)	R (mm)	c (mm)	S (mm^2)	r_2/R	I_{xx} (kg m^2)	I_{yy} (kg m^2)	I_{zz} (kg m^2)	I_{xz} (kg m^2)
88.88	0.560	11.2	2.98	33.34	0.550	5.23×10^{-13}	1.25×10^{-11}	1.20×10^{-11}	8.04×10^{-13}

m, insect mass; m_{wg}, mass of one wing; R, wing length; c, mean chord length of wing; S, area of one wing; r_2, radius of second moment of wing area; $I_{x,w}$, $I_{y,w}$, and $I_{z,w}$, moments of inertia of a wing about x_w, y_w and z_w axes, respectively; $I_{xz,w}$, product of inertia of a wing.

Table 2. Kinematical data of actual hovering

Φ (°)	n (Hz)	α_d (°)	α_u (°)	$\bar{\phi}$ (°)	θ_0 (°)	θ_1 (°)	Δt_r	β (°)	Re
107.1	164	34 (29.8)	33 (29.7)	7 (2.5)	4.0	3.0	0.3	0	782

Numbers in parentheses represent data modified to satisfy force and moment equilibrium conditions. Φ, the stroke amplitude; n, the stroke frequency; α_d, the angle of attack in downstroke translation; α_u, the angle of attack in upstroke translation; $\bar{\phi}$, the mean stroke angle; θ_0, the mean deviation angle, θ_1, the deviation amplitude; Δt_r, the wing rotation duration; β, the stroke plane angle; Re, Reynolds number.

If data in Tables 1 and 2 are directly used in the calculation of aerodynamic forces and power requirement, the forces acting on the insect might not be in balance, because there are necessarily errors in the measurement of the data. Here, we make small adjustment on the values of α_d, α_u, and $\bar{\phi}$, so that the flight is balanced, i.e., the vertical force being equal to the weight of the insect and the horizontal force and the pitch moment about the center of mass being equal to zero. The reason for only three parameters being modified is that there are three conditions to be met in hovering flight (zero mean horizontal force, mean vertical force balancing the weight, and zero mean pitch moment). The reason for choosing α_d, α_u, and $\bar{\phi}$ to be modified is that experimental data for α_d and α_u have relatively large error (Liu et al. 2008), and the aerodynamic forces and moments are very sensitive to the variations in α_d, α_u, and $\bar{\phi}$.

The adjustment of α_d, α_u, and $\bar{\phi}$ proceeds as follows. The original data of α_d, α_u, and $\bar{\phi}$ ($\alpha_d = 34°$, $\alpha_u = 33°$, and $\bar{\phi} = 7°$) are first used in the flow calculation and a set of mean vertical force ($\bar{V}$), mean horizontal force ($\bar{H}$), and mean pitch moment about center of mass ($\bar{N}$) are obtained. If $\bar{V}$ is not equal to the insect weight, or $\bar{H}$ and $\bar{N}$ are not equal to zero, α_d, α_u, and $\bar{\phi}$ are changed; the calculations are repeated until $\bar{V}$ is different from the insect weight, and $\bar{H}$ and $\bar{N}/c$ are different from zero by <3% of the insect weight. The modified values of α_d, α_u, and $\bar{\phi}$ are also given in Table 2 (values in parentheses).

Results and Discussion

Power Consumption in Actual Hovering. We first computed the power consumption in the actual hovering of the insect; i.e., we used the set of wing kinematical parameters that was actually employed by the insects (Table 2). The instantaneous aerodynamic ($C_{p,a}$), inertial ($C_{p,i}$), and total power (C_p) coefficients of a wing are given in Figure 4. It is interesting to note that the time course of C_p is more similar to that of $C_{p,i}$ than to that of $C_{p,a}$, because the inertial power is larger than the aerodynamic power in many part of the wing-beat cycle. This means that elastic energy storage could be important for the droneflies.

Integrating C_p over the part of a wing-beat cycle where it was positive gave the nondimensional positive work (C_w^+); integrating C_p over the part of a wing-beat cycle where it was negative gave the nondimensional negative work (C_w^-). Let C_w be the mean mechanical power over a wing-beat cycle. The mass-specific power (P^*) was determined as the mean mechanical power over a wing-beat cycle divided by the mass of the insect:

$$P^* = 0.5\rho U^3 \times (2S) \times (C_W/T)/m \quad (6)$$

where T was the wing-beat period. When calculating C_w, one needs to consider how the negative work fitted into the power budget. Ellington

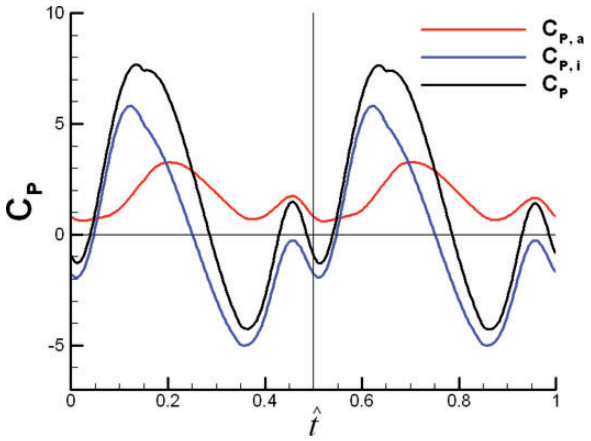

Fig. 4. The aerodynamic ($C_{p,a}$), inertial ($C_{p,i}$), and total power (C_p) coefficients of a wing in a wing-beat cycle at actual hovering.

(1984a, 1984b) suggested that there were three possibilities. One was that the negative power was simply dissipated as heat and sound by some form of an end stop, and then it could be ignored in the power budget. The second was that in the period of negative work, the excess energy could be stored by an elastic element, and this energy could then be released when the wing did positive work. The third was that the flight muscles did negative work (i.e., they were stretched while developing tension, instead of contracting as in "positive" work), but the negative work used much less metabolic energy than an equivalent amount of positive work, and again, the negative power could be ignored in the power budget. That is, out of these three possibilities, two ways of computing C_w could be taken. One is neglecting the negative work (zero elastic energy storage), i.e.,

$$C_w = C_w^+ \quad (7a)$$

The other is assuming that the negative work can be stored and released when the wing does positive work (100% elastic energy storage), i.e.,

$$C_w = C_w^+ - |C_w^-| = C_w^+ + C_w^- \quad (7b)$$

It should be noted that the inertial power in a complete cycle is exactly zero because the wing stroke is periodic; that is, the time average of $C_{p,i}$ in Figure 4 is zero. Thus, for the case of 100% elastic energy storage, C_w is only contributed by the $C_{p,a}$, the aerodynamic power.

There could be other possibilities; e.g., only certain amount of the negative work can be stored and released when the wing does positive work. We take 50% elastic energy storage as a forth possibility and an additional way of computing C_w is:

$$C_w = C_w{}^+ - 0.5|C_w{}^-| = C_w{}^+ + 0.5C_w{}^- \quad (7c)$$

With C_w computed by equations 7a, 7b, or 7c, the specific power P^* could be computed using equation 6. When C_w is computed by equations 7a, 7b, and 7c, the resulting P^* is denoted by P_1^*, P_2^*, and P_3^*, respectively. The computed results are as follows: P_1^*, P_2^*, and P_3^*, are 63.2, 52.4, and 41.5 W kg^{-1}, respectively. It is obvious that the power saving by elastic energy storage could be significant. The largest possible effect of elastic energy storage amounts to reduce the power by ~34%.

Power Consumption When Wing Kinematical Parameters Are Changed. In the section of "Power Consumption in Actual Hovering", power consumption in the case of actual hovering had been computed; i.e., wing kinematical parameters used in the computation were those actually employed by the hovering insect. Here, we change the kinematical parameters from the actual ones while keeping the equilibrium flight conditions satisfied and recalculate the power consumption.

The aerodynamic power in the midportion of a down- or upstroke is due to the wing drag and is mainly influenced by the lift-to-drag ratio of the wing (Sun and Tang 2002, Sun and Du 2003). Usherwood and Ellington (2002a, 2002b) measured the lift-to-drag ratios from mayfly to quail using rotating wings. Dickinson et al. (1999) measured lift-to-drag ratio of fruit fly wings, also using rotating-wing experiment. They showed that the lift-to-drag ratio of an insect wing was dependent on the angle of attack of wing; it decreased as angle of attack increased. From our computation, the lift-to-drag ratio of the dronefly wing can also be obtained, and it is shown in Figure 5. The lift-to-drag ratio decreases with angle of attack approximately linearly. Therefore, the aerodynamic power can be greatly influenced by α_d and α_u. The inertial power is mainly due to the translational acceleration of the wing (Sun and Tang 2002, Sun and Du 2003), which is proportional to Φn^2 (Sun and Du 2003). We thus see that power consumption is relatively sensitive to variations in Φ, n, α_d, and α_u. In this study, we would change the stroke amplitude (Φ), wing-beat frequency (n), and angle of attack (α_d and α_u); $\bar{\phi}$ is also adjusted to keep the equilibrium flight conditions satisfied. Note that because there are three conditions to be met for balanced flight (vertical force equals to the weight, and horizontal force and pitch moment are zero), only the variation of one of the four parameters (Φ or n, α_d, α_u, and $\bar{\phi}$) can be prescribed; variations of the other three parameters are determined by the equilibrium flight conditions. Here, we prescribed the variation of Φ or n and adjust α_d, α_u, and $\bar{\phi}$ based on equilibrium flight conditions. The process of adjusting α_d, α_u, and $\bar{\phi}$ has been described under *Flight Data*.

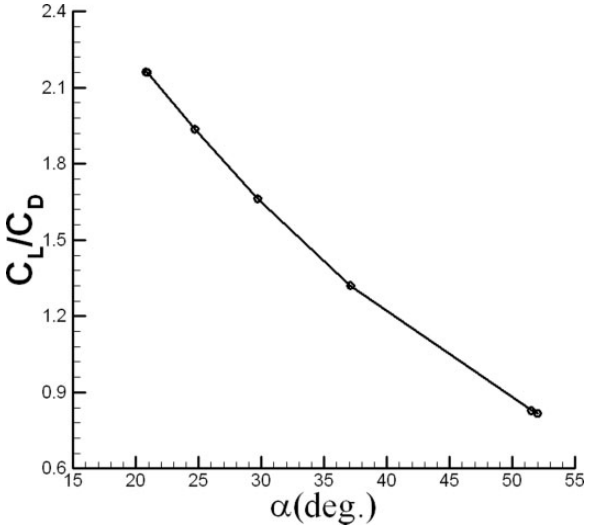

Fig. 5. The lift-to-drag ratio of the dronefly wing as a function of angle of attack.

Table 3 lists the prescribed Φ values and the corresponding values of α_d, α_u, and $\bar{\phi}$ that gave equilibrium flight (values of Φ, α_d, α_u, and $\bar{\phi}$ actually employed in the hovering flight are included for comparison). As given in the table, when Φ is increased or decreased from the value actually employed by the hovering insect, α_d and α_u decrease or increase ($\bar{\phi}$ changes only a little). This is because when Φ is increased (or decreased), the speed of the wing would be increased (or decreased), hence smaller (or larger) α_d and α_u are required to keep the vertical force unchanged.

Figure 6 shows the computed coefficients of aerodynamic ($C_{p,a}$), inertial ($C_{p,i}$), and total power (C_p) in a wing-beat cycle at various Φ (and the corresponding α_d, α_u, and $\bar{\phi}$). First, we examine the aerodynamic power coefficient $C_{p,a}$ (Fig. 6A). Let us first look at $C_{p,a}$ in the midportion of the down- and upstroke ($\hat{t} = 0.1 - 0.4$; $\hat{t} = 0.6 - 0.9$). When Φ is increased from the actual value ($\Phi = 107.1°$), $C_{p,a}$ decreases slightly, but when Φ is decreased, $C_{p,a}$ increases significantly. This is explained as follows. The slope of the curve of lift versus α of an insect wing becomes smaller and smaller as α is larger than 30° (Dickinson et al. 1999, Usherwood and Ellington 2002b, Wu and Sun 2004). In the actual hovering, α_d and α_u are already about 30° (Tables 2 and 3). When Φ is decreased from the actual value, α_d and α_u must have relatively large increase to produce enough lift because of the relatively small slope of the lift-versus-α curve at α larger than 30° (as Φ was decreased to 87°, α_d and α_u became 52° [Table 3]). Large α would produce large drag and small lift-to-drag ratio (as seen in Fig. 5, when α_d or α_u is 52° the lift-to-drag ratio is <2.8), resulting in the large increase in $C_{p,a}$. Let us now look at $C_{p,a}$ during the stroke reversal (Fig. 6A: $\hat{t} = 0.4 - 0.6$; and $\hat{t} = 0.9 - 1.0$ and $\hat{t} = 0 - 0.1$). Here, unlike the case of $C_{p,a}$ in the midportion of the down- and upstroke, as Φ is increased (or decreased), $C_{p,a}$ increases (or decreases). The reason for this is as follows. When Φ is increased (or decreased), α_d and α_u become smaller (or larger). Thus, the wing needs to rotate by a larger (or smaller) angle during stroke reversal, resulting a larger (or smaller) power.

Next, we examine at the inertial power coefficient $C_{p,i}$ (Fig. 6B). When Φ is increased or decreased from the actual value (107.1°), $C_{p,i}$ would increase or decrease (Fig. 6B). This is because a larger (or smaller) Φ gives larger (or smaller) translational acceleration of the wing.

Comparing $C_{p,a}$ (Fig. 6A) and $C_{p,i}$ (Fig. 6B) shown the following: when Φ is increased from the actual value, the change (increase) in $C_{p,i}$ is larger than the change (decrease) in $C_{p,a}$, hence the total power or specific power consumption would increase. When Φ is decreased from the actual value, first the change (increase) in $C_{p,a}$ is a little smaller, and then became larger, than the change (decrease) in $C_{p,i}$; as a result, the power consumption would first decrease slightly and then increase.

Figure 7 shows the computed specific power, P_1^*, P_2^*, and P_3^*. As expected, when Φ was increased (α_d and α_u decreased) from the actual

Table 3. Values of α_d, α_u and $\bar{\phi}$ determined by force and moment equilibrium conditions when Φ is varied

Φ (°)	α_d (°)	α_u (°)	$\bar{\phi}$ (°)
87.1	52.0	51.5	2.6
97.1	37.1	37.0	2.6
(107.1)	(29.8)	(29.7)	(2.5)
117.1	24.8	24.7	2.8
127.1	21.1	20.9	2.8

Values in the parentheses are those employed in the actual hovering flight. Φ, the stroke amplitude; α_d, the angle of attack in downstroke translation; α_u, the angle of attack in upstroke translation; $\bar{\phi}$, the mean stroke angle.

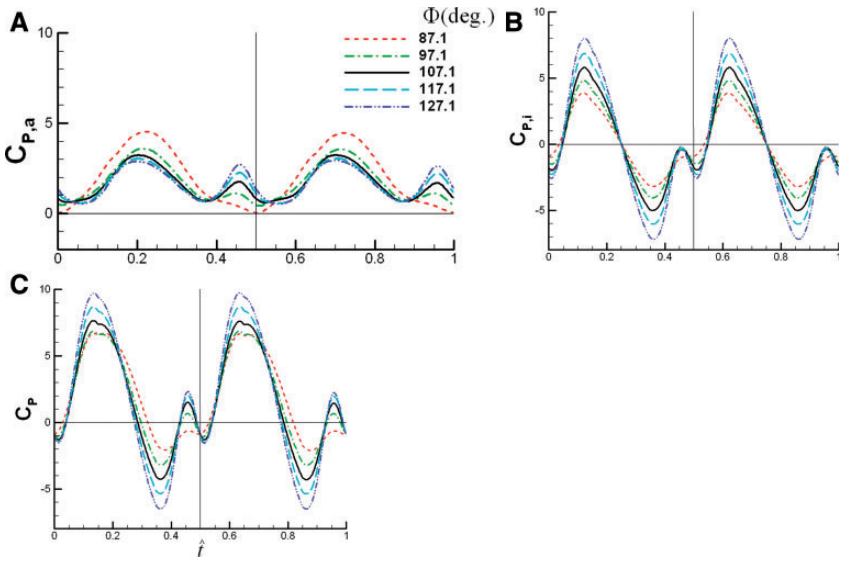

Fig. 6. The coefficients of aerodynamic ($C_{p,a}$), inertial ($C_{p,i}$), and total power (C_p) in a wing-beat cycle at various Φ values (and the corresponding values of α_d, α_u, and $\bar{\phi}$).

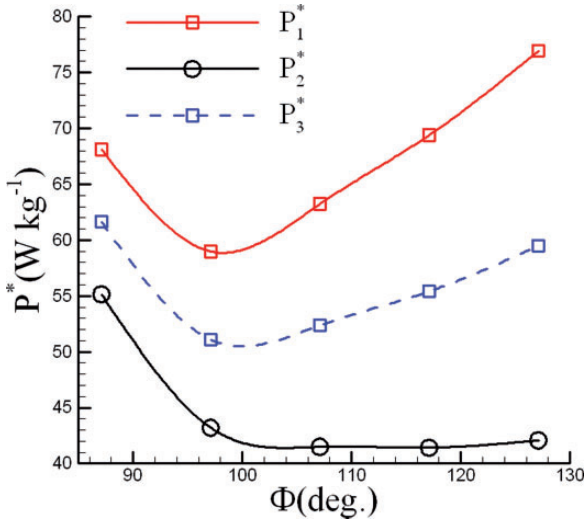

Fig. 7. The specific power, P_1^*, P_2^*, and P_3^*, at various Φ.

value, in general the specific power increased and when Φ was decreased (α_d and α_u increased) from the actual value, the specific power first decreased slightly and then increased rapidly.

The results for varying n (and α_d and α_u and $\bar{\phi}$) are given in Table 4 and Figures 8 and 9, which show the prescribed values of n (and the corresponding values of α_d, α_u and $\bar{\phi}$ for equilibrium flight), the power coefficients, and the specific power as a function of n, respectively. Explanation of these results is similar to that in the case of varying Φ.

For a real freely hovering dronefly, it was possible that the specific power was between P_1^* and P_2^* in Figures 7 and 9. This indicated that, on the one hand, wing kinematical parameters used by the freely hovering dronefly were very close to that minimize its energy consumption; on the other hand, these wing kinematical parameters could ensure the margin of controllability from hovering to maneuvers. That is, slight change of wing kinematical parameters did not cause significant change of the specific power (P^* maintained a relatively small value).

Some Discussions on the Assumptions Made in the Modeling. In the above calculations, we varied the stroke amplitude (Φ) or frequency (n), angle of attack (α_d and α_u), and mean positional angle of wing

Table 4. Values of α_d, α_u' and $\bar{\phi}$ determined by force and moment equilibrium conditions when n is varied

n (Hz)	α_d (°)	α_u (°)	$\bar{\phi}$ (°)
131.2	52.0	51.5	2.6
147.6	37.9	37.3	2.6
(164.0)	(29.8)	(29.7)	(2.5)
180.4	24.2	24.1	2.8
196.8	20.4	20.0	2.8

Values in the parentheses are those employed in the actual hovering flight. n, the flapping frequency; α_d, the angle of attack in downstroke translation; α_u, the angle of attack in upstroke translation; $\bar{\phi}$, the mean stroke angle.

subject to force and moment balance conditions. However, variations in other kinematical parameters, e.g., phase angle between wing stroke and pitching, elevation angle (θ), stroke plane angle (β), and the waveforms of Φ, α, and θ were not considered. Furthermore, the wings were assumed to be rigid. Some comments on these assumptions are given here.

The effect of varying phase angle between wing strokes and pitching on power requirement was investigated by Sun and Tang (2002). They showed that either an advanced or a delayed wing pitching would increase the power requirement. Symmetrical wing pitching, as that employed in this study, gave minimum power requirement. The effect of varying stroke plane angle on power requirement was considered by Mou et al. (2011). It was shown that changing β produce only very small change in power requirement. Thus, β being fixed at zero in this study should be reasonable.

The wings of most insects are corrugated, and in flapping motion, they undergo time-varying deformation. Walker et al. (2010) measured the time-varying deformation of wings in droneflies, and Rees (1975) measured the corrugation in droneflies and several other insects. Recently, Du and Sun (2012) studied the effects of wing deformation and corrugation on aerodynamic force and power of dronefly wings. They showed that when acting alone, wing deformation increases the lift and decreases aerodynamic power, but wing corrugation has opposite effects; when acting together, the effects of wing corrugation partially cancel that of the wing deformation. They concluded that using a rigid flat-plate wing to model the corrugated deforming dronefly wing is a good approximation.

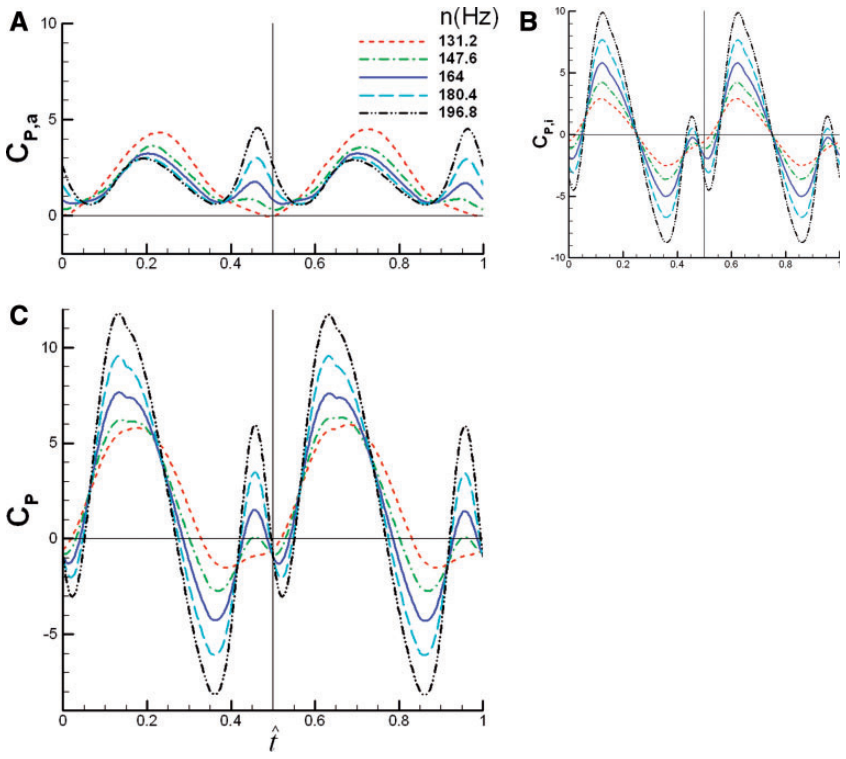

Fig. 8. The coefficients of aerodynamic ($C_{p,a}$), inertial ($C_{p,i}$), and total power (C_p) in a wing-beat cycle at various n values (and the corresponding values of α_d, α_u, and $\bar{\phi}$).

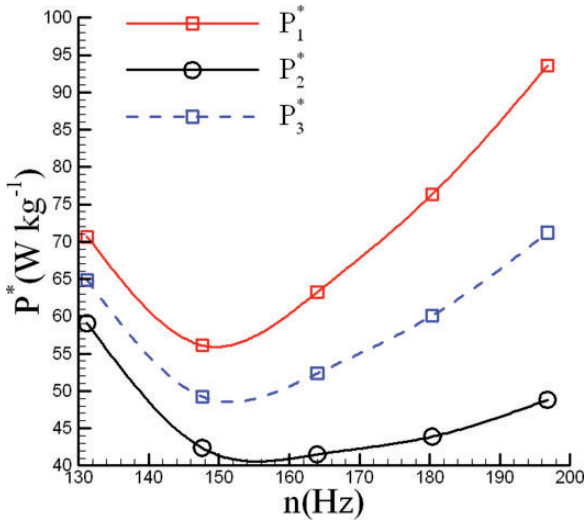

Fig. 9. The specific power, P_1^*, P_2^*, and P_3^*, at various n.

As far as we know, how changes in the amplitude of θ and in the waveforms of Φ, α, and θ would affect power requirements in equilibrium flight have not been investigated. Future work is required to investigate this.

When Φ or n was increased or decreased from the value actually employed by the hovering dronefly, α_d and α_u decreased or increased ($\bar{\phi}$ changed a little) to keep the equilibrium flight conditions satisfied. When Φ or n was increased (α_d and α_u decreased) from the actual value, in general the specific power increased and when Φ or n was decreased (α_d and α_u increased), the specific power first decreased slightly and then increased. Therefore, it could be said that wing kinematical parameters used by the freely hovering dronefly were very close to that minimize its energy consumption, and they could ensure the margin of controllability from hovering to maneuvers. That is, slight change of wing kinematical parameters did not cause significant change of the specific power (P^* maintained a relatively small value).

Acknowledgments

This research was supported by grants from the National Natural Science Foundation of China (11232002) and the Foundation for Author of National Excellent Doctoral Dissertation of China (2007B31).

References Cited

Aono, H., F. Liang, and H. Liu. 2008. Near- and far-field aerodynamics in insect hovering flight: and integrated computational study. J. Exp. Biol. 211: 239–257.

Dickinson, M. H., F. O. Lehman, and S. P. Sane. 1999. Wing rotation and the aerodynamic basis of insect flight. Science 284: 1954–1960.

Du, G., and M. Sun. 2012. Aerodynamic effects of corrugation and deformation in flapping wings of hovering hoverflies. J. Theor. Biol. 300: 19–28.

Dudley, R., and C. P. Ellington. 1990. Mechanics of forward flight in bumblebees. II. Quasi-steady lift and power requirements. J. Exp. Biol. 148: 53–88.

Ellington, C. P. 1984a. The aerodynamics of hovering insect flight. II. Morphological parameters. Philos. Trans. R. Soc. Lond. B 305: 17–40.

Ellington, C. P. 1984b. The aerodynamics of hovering insect flight. VI. Lift and power requirements. Philos. Trans. R. Soc. Lond. B 305: 145–181.

Fry, S. N., R. Sayaman, and M. H. Dickinson. 2005. The aerodynamics of hovering flight in *Drosophila*. J. Exp. Biol. 208: 2303–2318.

Liu, H., and H. Aono. 2004. Size effects on insect hovering aerodynamics: an integrated computational study. Bioinspir. Biomim. 4: 015002.

Liu, Y.P. and M. Sun. 2008. Wing kinematics measurement and aerodynamics of hovering droneflies. J. Exp. Biol. 211: 2014–2025.

Mou, X. L., Y. P. Liu, and M. Sun. 2011. Wing motion measurement and aerodynamics of hovering true hoverflies. J. Exp. Biol. 214: 2832–2844

Rees, C. J. C. 1975. Aerodynamic properties of an insect wing section and a smooth aerofoil compared. Nature 258: 141–142.

Sun, M., and G. Du. 2003. Lift and power requirements of hovering insect flight. Acta Mech. Sin. 19: 458–469.

Sun, M., and J. Tang. 2002. Lift and power requirements of hovering flight in *Drosophila*. J. Exp. Biol. 205: 2413–2427.

Usherwood, J. R., and C. P. Ellington. 2002a. The aerodynamics of revolving wings. I. Model hawkmoth wings. J. Exp. Biol. 205: 1547–1564.

Usherwood, J. R., and C. P. Ellington. 2002b. The aerodynamics of revolving wings. II. Propeller force coefficients from mayfly to quail. J. Exp. Biol. 205: 1565–1576.

Walker, S. M., A. L. R. Thomas, and G. K. Taylor. 2010. Deformable wing kinematics in free-flying hoverflies. J. R. Soc. Interface 7: 131–142.

Wu, J. H., and M. Sun. 2004. Unsteady aerodynamic forces of a flapping wing. J. Exp. Biol. 207: 1137–1150.

Wu, J. H., Y. L. Zhang, and M. Sun. 2009. Hovering of model insects: simulation by coupling equations of motion with Navier–Stokes equations. J. Exp. Biol. 212: 3313–3329.

Yu, X., and M. Sun. 2009. A computational study of the wing-wing and wing-body interactions of a model insect. Acta Mech. Sin. 25: 421–431.

Zhao, L., and X. Deng. 2009. Power distribution in the hovering flight of the hawk moth *Manduca sexta*. Bioinspir. Biomim. 4: 046003.

Received 25 December 2012; accepted 16 September 2013.